To determine the change in the slipstream shape due to the centrifugal terms, the pressure relation is rewritten, neglecting the static pressure terms which are important only in the tail region, as follows

$$d\sigma/d\theta = \sin^j\theta[R\cos^2\sigma - \cos^2(\theta - \sigma)]/g(\theta)\cos(\theta - \sigma) \quad (20a)$$

where

$$dg/d\theta = \sin^j\theta[R\sin 2\sigma + \sin 2(\theta - \sigma)]/2\cos(\theta - \sigma) \quad (20b)$$

and

$$R = r^{j+1} \quad (20c)$$

$$dy = [r\cos\sigma/\cos(\theta - \sigma)]d\theta \quad (20d)$$

has been substituted. Here $g(\theta)$ represents the growth of the tangential momentum in the shock layers. The preceding equation shows that the slipstream curvature is proportional to the ratio of the difference in the normal component of the dynamic pressure to the tangential momentum.

The geometric condition

$$dR/d\theta = (j + 1)R\tan(\theta - \sigma) \quad (20e)$$

together with the initial conditions at

$$\theta = 0, \quad \sigma = 0, \quad R = 1, \quad g = 0 \quad (20f)$$

form a system of three nonlinear ordinary differential equations for the three unknowns σ, R, g.

For the two-dimensional source $j = 0$, the aforementioned system admits a simple solution

$$\sigma = \theta/2 \quad (21)$$

This implies the curvature factor $d\sigma/d\theta$ is a constant. The geometric condition gives

$$\bar{r} = 1/\cos^2(\theta/2) \quad (22)$$

and integration of the tangential momentum growth equation yields

$$g(\theta) = 2\tan(\theta/2)\sin(\theta/2) \quad (23)$$

For the spherical source a series solution is obtained for $\theta \ll 1$ by noting that due to symmetry

$$R = 1 + R_0''\theta^2/2! + R_0''''\theta^4/4! + \ldots \quad (24)$$

and

$$\sigma = \sigma_0'\theta + \sigma_0'''\theta^3/3! + \ldots \quad (25)$$

in which the primes denote differentiation with respect to theta. Here σ_0' is recognized to be the curvature of the slipstream at the centerline. Substituting these expansions into the differential equation for g and integrating gives

$$g(\theta) = \theta^{j+2}/(j + 2) - (\sigma_0'R_0'' - \tfrac{1}{3}\sigma_0'^3 - \tfrac{4}{3} + 3\sigma_0' - 3\sigma_0'^2)\theta^{j+3}/2(j + 3) + \tfrac{1}{2}(1 - 2\sigma_0' + \sigma_0'^2 - j/3)\theta^{j+4}/(j + 4) + \ldots \quad (26)$$

The differential equation for the curvature evaluated at $\theta = 0$ gives

$$\sigma_0' = (j + 2)(R_0'' + 2)/2(2j + 5) \quad (27)$$

The geometric condition differentiated once and evaluated at $\theta = 0$ gives

$$R_0'' = (j + 1)(1 - \sigma_0') \quad (28)$$

From which

$$\sigma_0' = (j + 2)/(j + 4) \quad (29)$$

and

$$R_0'' = 2(j + 1)/(j + 4) \quad (30)$$

The series solution for $\bar{r}$ and σ become

$$\bar{r} = 1 + [1/(j + 4)]\theta^2 + \ldots \quad (31)$$

$$\sigma = (j + 2)/(j + 4)\theta + \ldots \quad (32)$$

A numerical integration of this system was obtained with the help of a CDC 6600 computer. Numerical accuracy of 0.01% was imposed at each integration step by using Runge-Kutta integration with variable step size. The results of this computation are shown graphically on Fig. 2 along with the analytic solution and the series expansion.

The slipstream shapes differ significantly for theta greater than approximately one radian by the inclusion or deletion of the centrifugal terms. This departure is largely due to increasing tangential momentum in the shock layers and not so much to the curvature of the slipstream.

References

[1] Hayes, W. D. and Probstein, R. F., *Hypersonic Flow Theory*, Academic Press, New York, 1959, p. 78.

[2] Milne-Thomson, L. M., *Theoretical Hydrodynamics*, Macmillan, New York, 1955.

[3] Prandtl, L. and Tietjens, O. G., *Fundamentals of Hydro- and Aeromechanics*, Dover, New York, 1957, p. 147.

Experimental Investigation of the Lee-Side Flow from a Cone-Cylinder Model

Alfred M. Morrison* and Charles W. Ingram†
University of Notre Dame, Notre Dame, Ind.

Introduction

One phase of the general problem of the interference between component parts of flight vehicles is the interference effects resulting from vortex shedding from a body of revolution at high angles of attack. When the angle of attack is small the boundary layer beings to thicken rapidly on the lee side of the body near the base. As the angle of attack or length fineness ratio is increased this phenomena progresses until the boundary layer separates from the body and two regions of concentrated vorticity are formed on the lee side. At this point the influences of inertia and viscosity of the air flowing around the body can no longer be neglected. The formation of the vortices results in a pressure reduction which increases the cross forces substantially more than potential flow theory would lead one to believe. Wind-tunnel tests have shown that these vortices have a large effect upon the forces developed on wing and tail surfaces.[1] Certain methods exist for estimating the forces developed on the wing and tail surfaces provided the positions and strengths of the body vortices are known.[1-4] The purpose of this Note is to present an experimental method for determining the position of the vortex core regions from subsonic wind-tunnel tests.

Experimental Procedure

The smoke flow visualization techniques of Brown[5] were used in this investigation. In order to obtain proper visualization of the flow, a converging slit-camera technique was employed. A schematic representation of this process is presented in Fig. 1. The technique employed two wind-

Received January 11, 1971; revision received February 16, 1971.

* Graduate Student, Research Assistant. Associate Member AIAA.

† Assistant Professor of Aerospace and Mechanical Engineering. Member AIAA.

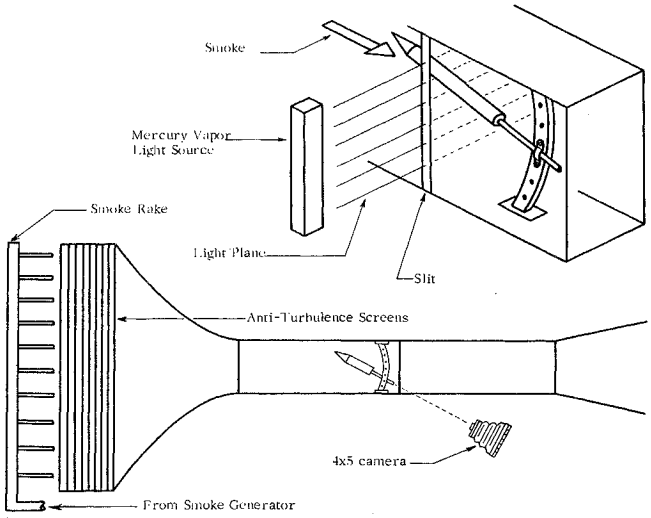

Fig. 1 Schematic of test equipment.

tunnel working sections. The forward working section has a removable back wall and a glass front wall to allow for illumination of the model. The aft section had three glass walls to allow for visual observation of the flowfield in a plane perpendicular to the symmetric axis z of the model. A still camera was used to photograph the smoke flow through the glass floor of the aft section. The smoke vortices were photographed at four different body positions. To insure repeatability of the data, two runs were made at each body position. This process was carried out at four different angles of attack. Two luminous reference dots were fixed to a thin wire passing through the support sting of the model to determine the positions of the vortices. Corrections of the photographic data were made for apparent distance changes when the reference dots were projected into the plane of the smoke vortices. All tests were conducted at a tunnel velocity of 28.4 fps.

Discussion of Results

The primary objective of the test program was to develop a method by which the vortex core region could be located at various body positions for various angles of attack. The photographic quality of the smoke visualization is determined by the nature of the lighting system. It was necessary to use a slit 0.1 in. in width and 3 in. in depth in conjunction with a high-intensity light source in order to obtain a light plane of acceptable width and photographic intensity. An optical comparator system was used to locate the vortex core area by measuring points along the edge of the dark core region. A

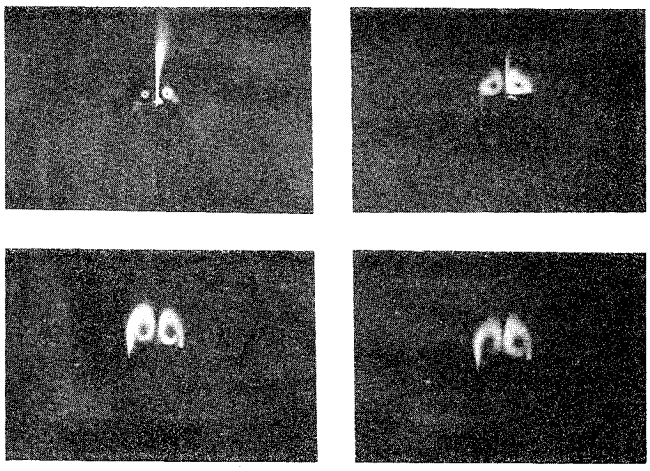

Fig. 2 Smoke photography of core locations reading left to right.

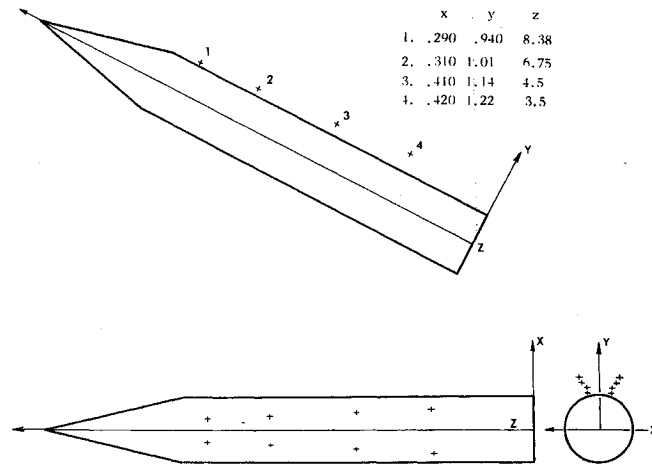

Fig. 3 Core center locations for $\alpha = 27.0°$.

computer program was then used to convert the comparator readings to inches and to assign them values relative to the center of the cone cylinder configuration. Because of the apparent shape of the vortex core regions, ellipses were fit to the data and the center of the ellipse was taken to be the center of the vortex core region. Example photographs of the smoke visualizations are presented in Fig 2. The smoke is seen as the white portions of the photographs, while the black oval centers of the smoke are representative of the vortex core areas. A vertical line of smoke is noted on many of the photographs such as shown in Fig. 2. The vertical line is representative of smoke which was not diffused into the wake region. Rings of smoke were also noted as shown in Fig. 2. Such rings are formed when smoke enters the flowfield at a forward point on the cone cylinder configuration where the vortex is actually forming. Figure 3 gives the vortex core locations in inches from the tail, at angle of attack α equal to 27° as shown in Fig. 2. Variations in height above the cone cylinder configuration are presented on the profile view, while radial variations are presented on the end view. The plot shown is representative of the data shown in Table 1 and repeatability was found to be good for all runs. As the body position of the vortex core region moves toward the rear of the cone cylinder, the height of the core region center was found to increase. Symmetry of the core region centers about an axis passing through the center of the test configuration was found to be distorted for angle of attack of 35° at the two most rearward body positions. This would be representative of the beginning of an asymmetric condition of the wake. The occurrence of this phenomenon at this point is in good agreement with the data of Ref. 6. Reference 6 suggests

Table 1 Vortex core center locations

	$\alpha = 22.5°$				$\alpha = 27.0°$		
	x	y	z		x	y	z
1)	0.275	0.900	8.31	1)	0.290	0.940	8.38
2)	0.285	0.990	6.75	2)	0.310	1.01	6.75
3)	0.430	1.19	4.50	3)	0.410	1.14	4.50
4)	0.340	1.10	3.50	4)	0.420	1.22	3.50
	$\alpha = 31.0°$				$\alpha = 35.0°$		
	x	y	z		x	y	z
1)	0.275	1.00	8.38	1)	0.285	0.910	8.25
2)	0.320	1.10	6.75	2)	0.370	0.980	6.75
3)	0.395	1.20	4.50	3)	0.405	1.32	4.50
4)	0.440	1.30	3.50	[a]	0.405	1.24	4.50
				4)	0.425	1.49	2.50
				[a]	0.425	1.40	2.50

[a] Denotes asymmetrical core center locations.

that the vortex core region centers move radially outward along a line at an angle of 67° from a horizontal axis passing through the center of the test configuration. The data taken here were not found to exhibit such a trent. The core region center moves radially outward along a line curving away from the center of the test configuration. The outward curve becomes sharper as the angle of attack is increased. This trend is exactly opposite to the supersonic case as reported in Ref. 7. That is, in the supersonic case the core region centers were found to first move radially outward then to move along a line curving slightly back toward the center of the test configuration.

References

[1] Mello, J. F., "Investigation of Normal Force Distribution and Wake Vortex Characteristics of Bodies of Revolution at Supersonic Speeds," CM 867, April 1956, Johns Hopkins Univ., Baltimore, Md.

[2] Mello, J. F., "Investigation of Normal Force Distribution and Wake Vortex Characteristics of Bodies of Revolution at Supersonic Speeds," *Journal of the Aerospace Sciences*, Vol. 26, No. 1, Jan. 1959, pp. 155–168.

[3] Oberkampf, W. L., "Prediction of Forces and Moments on a Finned Missile at High Angle of Attack," Ph.D. dissertation, Aug. 1970, Univ. of Notre Dame, Notre Dame, Ind.

[4] Tobak, M., Schiff, S. B., and Petersen, V. L., "Aerodynamics of Bodies of Revolution in Nonplanar Motion," AIAA Paper 68-20, New York, 1968.

[5] Brown, F. N. M. and Poynton, J. P., "Associated Force and Flow Study on an Ogive Nose Cylinder," AS-107, June 1958, Dept. of Aerospace and Mechanical Engineering, Univ. of Notre Dame, Notre Dame, Ind.

[6] Feichter, M., "On the Vortex System of High Fineness Ratio Bodies of Revolution and Their Influence on the Aerodynamic Coefficients," translation from German by W. L. Oberkampf and M. Prokop, AS-1021, Aug. 1969, Dept. of Aerospace and Mechanical Engineering, Univ. of Notre Dame, Notre Dame, Ind.

[7] Jorgensen, L. and Perkins, E. W., "Investigation of Some Wake Vortex Characteristics of an Inclined Ogive-Cylineer Body at Mach Number 1.98," Rm A55E31, Aug. 1955, NACA.

A New Integral Calculation of Skin Friction on a Porous Plate

TSE-FOU ZIEN*
U. S. Naval Ordnance Laboratory, Silver Spring, Md.

Nomenclature

C_f = skin-friction coefficient, $\tau_w/\frac{1}{2}\rho u_0^2$
f = velocity profile, u/u_0
k = coefficients of the polynomial velocity profiles
Re_x = Reynolds number based on distance x, $u_0 x/\nu$
Re_δ = Reynolds number based on boundary-layer thickness, $u_0\delta/\nu$
(u,v) = velocity components corresponding to (x,y)
(x,y) = Cartesian coordinate system with origin at the leading edge, x along the freestream direction
$\alpha = \int_0^1 f d\eta - \int_0^1 f^2 d\eta - \int_0^1 f d\eta \int_0^\eta f d\eta + \int_0^1 d\eta \int_0^\eta f^2 d\eta$
$\beta = 1 - \int_0^1 f d\eta$
$\gamma = \int_0^1 f d\eta - \int_0^1 f^2 d\eta$
δ = boundary-layer thickness
ϵ = blowing parameter, v_w/u_0
η = similarity variable, y/δ
λ = blowing parameter, $(v_w/u_0)\,(x/\delta)$
$\tilde{\lambda}$ = blowing parameter, $(v_w/u_0)\,(Re_x^{1/2})$
ν = kinematic viscosity
ρ = density of the fluid
τ = shear stress

Subscripts

0 = freestream condition
w = wall

Received January 21, 1971. This research was supported by NOL Independent Research program.

* Research Aerospace Engineer, Applied Aerodynamics Division. Member AIAA.

Introduction

THIS Note reports on some preliminary results for the incompressible, laminar skin friction on a porous plate calculated by a refined Karman-Pohlhausen (K-P) method. Only two types of surface blowing (or suction) are considered, namely, the similarity type for which $v_w \sim x^{-1/2}$ and the uniform type for which v_w = constant. Exact numerical results exist for both cases so that the capability of this new method can be tested. It will be revealed that remarkably accurate and reliable results can be obtained in analytic forms, requiring only simple and elementary calculations.

Volkov[1] recently advanced the basic idea of the refined K-P method, and a slight modification is made here to generalize application to flows over permeable surfaces in order to assess its validity in general boundary-layer flows including the effects of surface mass transfer. In essence, the method is based on a double integration of boundary-layer equations in the direction normal to the external main stream. The skin-friction term can thus be expressed in terms of certain integrals of the assumed velocity profile instead of the derivative of it, as in the usual K-P method. One expects that the accuracy of the skin-friction, so expressed, should be significantly increased and that, as a consequence, the method should yield improved results in cases where the skin friction plays an important role, such as boundary-layer flows pertinent to separation.

Analysis

We begin with the integrated version of the laminar boundary-layer equations over a porous plate, i.e.,

$$\frac{\partial}{\partial x}\int_0^y u^2 dy + uv = \nu\frac{\partial u}{\partial y} - \frac{\tau_w(x)}{\rho} \tag{1}$$

Note that Eq. (1) with the upper limit of the integral replaced by $\delta(x)$ is the familiar K-P equation for the determination of $\delta(x)$. However, following the idea of Volkov's refinement,[1] we shall use this equation as an expression for the skin friction, $\tau_w(x)$. The quantity $\delta(x)$ will then be determined by an equation obtained by another integration of Eq. (1). Thus the ordinary differential equation determining the basic quantity $\delta(x)$ is

$$\int_0^\delta dy \frac{\partial}{\partial x}\int_0^y u^2 dy + v_w\int_0^\delta u dy - \int_0^\delta u dy \frac{\partial}{\partial x}\int_0^y u dy = \nu u_0 + \delta\frac{d}{dx}\int_0^\delta u^2 dy + \delta u_0 v_w - \delta u_0 \frac{d}{dx}\int_0^\delta u dy \tag{2}$$

Note that in arriving at Eq. (2), we have substituted for $\tau_w(x)$ an expression derived from Eq. (1), i.e.,

$$\frac{1}{2}C_f \equiv \frac{\tau_w(x)}{\rho u_0^2} = \frac{d}{dx}\int_0^\delta \frac{u}{u_0}\left(1 - \frac{u}{u_0}\right)dy - \epsilon \tag{3}$$

Eqs. (2) and (3) form the basis of the ensuing calculations.

As for the velocity profiles to be used in Eq. (2), we shall adopt the familiar form of polynomials with constant coefficients, i.e., we assume

$$u/u_0 = f(\eta) = \Sigma_i k_i \eta^i, \quad k_i = \text{const} \tag{4}$$